Root responses to aluminium and iron stresses require the SIZ1 SUMO ligase to modulate the STOP1 transcription factor

Caroline Mercier[1,2], Brice Roux[1], Marien Have[1], Léa Le Poder[1], Nathalie Duong[1], Pascale David[1], Nathalie Leonhardt[1], Laurence Blanchard[3], Christin Naumann[4], Steffen Abel[4], Laura Cuyas[2], Sylvain Pluchon[2], Laurent Nussaume[1] and Thierry Desnos[1,*] (ID)

[1]*Aix Marseille Univ, CEA, CNRS, BIAM, UMR7265, SAVE, Saint Paul-Lez-Durance 13108, France,*
[2]*Laboratoire de Nutrition Végétale, Agroinnovation International—TIMAC AGRO, Saint-Malo, France,*
[3]*Aix Marseille Univ, CEA, CNRS, BIAM, UMR7265, MEM, Saint Paul-Lez-Durance 13108, France, and*
[4]*Department of Molecular Signal Processing, Leibniz Institute of Plant Biochemistry, Halle (Saale) 06120, Germany*

SUMMARY

STOP1, an Arabidopsis transcription factor favouring root growth tolerance against Al toxicity, acts in the response to iron under low Pi (−Pi). Previous studies have shown that Al and Fe regulate the stability and accumulation of STOP1 in roots, and that the STOP1 protein is sumoylated by an unknown E3 ligase. Here, using a forward genetics suppressor screen, we identified the E3 SUMO (small ubiquitin-like modifier) ligase SIZ1 as a modulator of STOP1 signalling. Mutations in *SIZ1* increase the expression of *ALMT1* (a direct target of STOP1) and root growth responses to Al and Fe stress in a STOP1-dependent manner. Moreover, loss-of-function mutations in *SIZ1* enhance the abundance of STOP1 in the root tip. However, no sumoylated STOP1 protein was detected by Western blot analysis in our sumoylation assay in *Escherichia coli*, suggesting the presence of a more sophisticated mechanism. We conclude that the sumo ligase SIZ1 negatively regulates STOP1 signalling, at least in part by modulating STOP1 protein in the root tip. Our results will allow a better understanding of this signalling pathway.

Keywords: SIZ1, SUMO, STOP1, ALMT1, aluminium, iron, phosphate, root, Arabidopsis.

INTRODUCTION

STOP1 (SENSITIVE TO PROTON RHIZOTOXICITY1) is an Arabidopsis C_2H_2 transcription factor that regulates the expression of several genes involved in plant growth responses to various environmental cues (Daspute et al., 2017).

This gene was first discovered because of its role in roots in resisting low rhizospheric pH; subsequently, it was found that *stop1* knockout (KO) mutants are also very sensitive to aluminium (Iuchi et al., 2007). Sensitivity to aluminium toxicity was then shown to be mostly due to the lack of expression of *ALMT1* (*ALUMINUM-ACTIVATED MALATE TRANSPORTER 1*) and also *MATE* (MULTIDRUG AND TOXIN EXTRUSION), encoding root transporters that exude malate and citrate, respectively (Hoekenga et al., 2006; Iuchi et al., 2007; Kobayashi et al., 2007; Liu et al., 2009; Sawaki et al., 2009). These small organic acids can form complexes with Al^{3+}, thereby preventing its toxicity (Kochian et al., 2015; Figure 1).

STOP1 positively regulates the expression of other genes such as *ALS3* (*ALUMINUM SENSITIVE3*), *GDH1* and *GDH2* (*GLUTAMATE-DEHYDROGENASE1* and *2*) also participating in Al tolerance, and of *RAE1* (*REGULATION OF AtALMT1 EXPRESSION1*; Sawaki et al., 2009; Tokizawa et al., 2021; Zhang et al., 2019b).

Several studies have shown that low-Pi growth medium (−Pi) also inhibits the primary root growth of wild-type (WT) Arabidopsis seedlings (Abel, 2017; Gutiérrez-Alanís et al., 2018; Niu et al., 2013). This short root phenotype is due to the inhibition of cell expansion and proliferation. This growth inhibition is prevented by reducing iron concentration, either by lowering the iron concentration in the growth media or by its chelation of iron with deferoxamine (Balzergue et al., 2017; Godon et al., 2019; Mora-Macías et al., 2017; Muller et al., 2015; Svistoonoff et al., 2007). Thus, the −Pi condition inhibits root growth via the presence of rhizospheric iron cations (Figure 1).
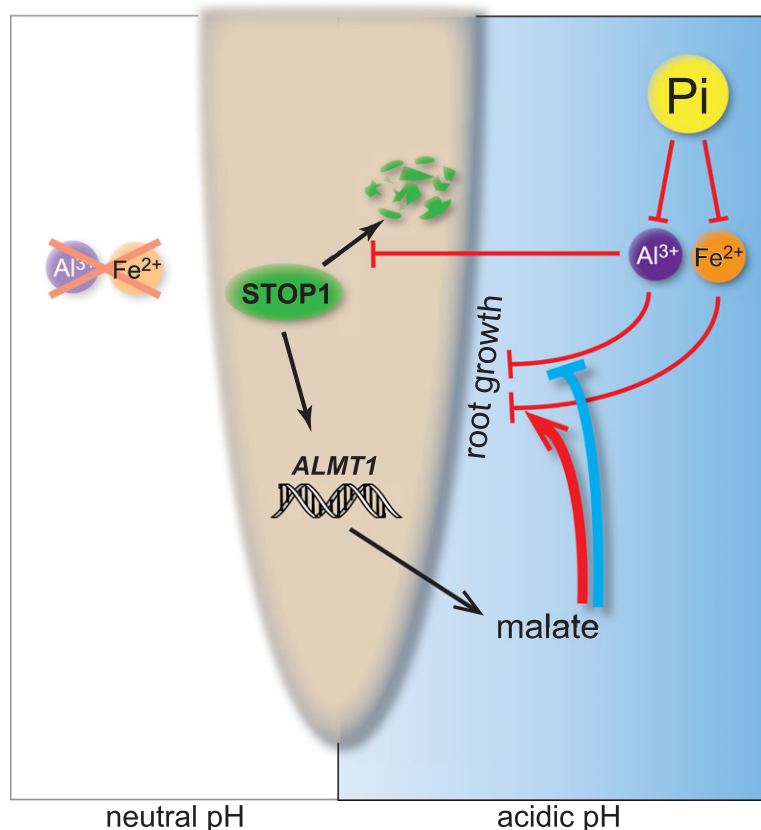
Figure 1. Simplified diagram summarizing the environmental conditions and STOP1-dependent signalling affecting Arabidopsis root growth.
Under acidic conditions (right side), aluminium and iron ions inhibit the proteasome-dependent degradation of the STOP1 protein, thereby increasing the expression of *ALMT1* and the exudation of malate. When combined with malate, iron inhibits root growth (red arrow), whereas malate prevents aluminium toxicity (blue blunt arrow). Phosphate chelates metallic ions, thereby decreasing their detrimental effect on root growth. Under neutral pH (left side), Al and Fe ions do not inhibit root growth or prevent STOP1 degradation.

A number of studies have used genetic screens to identify genes involved in this growth response to −Pi, including *STOP1* and *ALMT1* (Abel, 2017; Balzergue et al., 2017; Gutiérrez-Alanís et al., 2017, 2018; Mora-Macías et al., 2017; Muller et al., 2015; Svistoonoff et al., 2007; Ticconi et al., 2009; Wang et al., 2019). Recently, it was discovered that the primary root growth of *stop1* and *almt1* mutants is more resistant to the inhibitory effect of Fe ions under −Pi (Balzergue et al., 2017; Mora-Macías et al., 2017). The long primary root phenotype of *stop1* is due to the lack of expression of *ALMT1* in the root tip. Thus, the lack of malate (which could otherwise interact with Fe cations outside of the root cells) together with the ferroxidase LPR1 is thought to generate reactive oxygen species that inhibit cell wall expansion. We previously showed that the constitutive expression of *ALMT1* complements the root response to −Pi in the *stop1* mutant (Balzergue et al., 2017). Therefore, under −Pi, STOP1-ALMT1 signalling in roots is crucial for responding to Fe. Furthermore, several previous reports indicate that the contrasting responses of primary root growth to Al^{3+} and −Pi (Fe) have become a popular readout for STOP1 activity when studying STOP1 signalling (Fang et al., 2020, 2021b; Guo et al., 2020; Mora-Macías et al., 2017; Zhang et al., 2019b).

Recently, we demonstrated by confocal microscopy that, under −Pi, the stability of the GFP-STOP1 fusion protein in the nuclei of root cells is highly dependent on the presence of Al or Fe, as well as pH. We also showed that ALS3 and STAR1 (SENSITIVE TO ALUMINUM RHIZOTOXICITY1), which together form a tonoplast-located ABC transporter complex for an unknown substrate, negatively modulate the abundance of STOP1 (Godon et al., 2019; Wang et al., 2019). GFP-STOP1 accumulates in nuclei under low pH, as well as when Al or Fe ions are present in micromolar ranges (Figure 1). In contrast, conditions that can inhibit STOP1 accumulation include a neutral pH, or the absence of Al and Fe. The pharmacological inhibition of the proteasome strongly enhances the accumulation of nuclear GFP-STOP1 in growth conditions where this protein poorly accumulates (Godon et al., 2019). The stability of STOP1 in root cells therefore appears to be a major regulatory step in controlling STOP1 signalling in response to rhizospheric cues. The Al-induced nuclear accumulation of STOP1 was recently confirmed in +Pi conditions, even in the presence of a protein synthesis inhibitor, suggesting the post-translational regulation of STOP1 (Tokizawa et al., 2021).

In a recent forward genetic screen of a WT Arabidopsis line expressing a luciferase marker driven by the *ALMT1* promoter, RAE1 was identified as a regulator of STOP1

stability (Zhang et al., 2019b). RAE1 encodes an E3 ubiquitin ligase and, compared with WT, *rae1* mutants accumulate more STOP1 protein and show stronger expression of the *ALMT1*, *MATE* and *ALS3* genes. These data correlate with the enhanced resistance of these seedlings to toxic Al^{3+} and an enhanced sensitivity to $-Pi$ medium (Zhang et al., 2019b).

Like ubiquitin, SUMO (SMALL UBIQUITIN-LIKE MODIFIER) is a small eukaryotic protein that can be covalently attached (or 'tagged') to lysine residues on a target protein. Several differentially expressed isoforms of SUMO proteins exist in Arabidopsis (SUMO1, SUMO2, SUMO3 and SUMO5), and the highly similar SUMO1 and SUMO2 are both predominant and together essential (Augustine and Vierstra, 2018; Saracco et al., 2007). Sumoylation, the tagging of a protein substrate by one or more SUMO tags, participates in the fate of the target by modulating its activity or changing its subcellular location (Flotho and Melchior, 2013). Proteomic analyses in Arabidopsis have shown that hundreds of proteins are targets of sumoylation, although the molecular functions of most of these sumoylations are not known (Elrouby and Coupland, 2010; Miller et al., 2010, 2013; Rytz et al., 2018).

In cells, a SUMO tag can be removed from its protein substrate by SUMO proteases. There are eight genes in Arabidopsis that encode ubiquitin-like proteases (ULPs), including *ESD4* (Benlloch and Lois, 2018; Novatchkova et al., 2012). ESD4 was identified in the same genetic screen that identified the ubiquitin ligase RAE1 as a regulator of STOP1 (Zhang et al., 2019b). STOP1 was subsequently discovered as the first substrate of ESD4, which physically interacts with STOP1 and desumoylates sumoylated STOP1 (Fang et al., 2020). Moreover, plants homozygous for *esd4* mutations accumulate more sumoylated STOP1. In addition, the expression of *ALMT1* is higher in *esd4* seedlings than in the WT. These mutants therefore display a moderate (although significantly increased) resistance to Al^{3+} as well as sensitivity to $-Pi$ conditions (Fang et al., 2020).

While ESD4 desumoylates STOP1, it remains unknown which protein catalyses STOP1 sumoylation. In Arabidopsis, several protein catalysts mediate sumoylation in three successive steps: SAE2 and SAE1 (isoform SAE1a or SAE1b) activate SUMO, which is then transferred to SCE1, and finally conjugated to protein substrates. The final conjugation step can be facilitated in some cases by a SUMO ligase (SIZ1, MMS21/HPY2 or PIAL1/2; Augustine and Vierstra, 2018; Benlloch and Lois, 2018).

The role of Arabidopsis SIZ1 was initially described in Pi starvation-dependent responses (Miura et al., 2005). The *siz1* KO mutations exacerbate seedling growth responses to Pi limitation, including reduced primary root growth (Miura et al., 2005). Visual reporters of auxin signalling indicate that Pi starvation induces modifications of auxin patterns in roots earlier in the *siz1* mutant than in the WT (Miura et al., 2011).

At the molecular level, *siz1* mutations both positively and negatively alter some target genes of *PHR1* (*PHOSPHATE STARVATION RESPONSE 1*), a master regulator of Pi homeostasis (Bustos et al., 2010; Rubio et al., 2001). In addition, SIZ1 sumoylates PHR1 both *in vivo* (Miller et al., 2010) and *in vitro* (Miura et al., 2005). These findings suggest that SIZ1 has a complex role in responses to Pi limitation.

Since its first described role in $-Pi$, SIZ1 has been found to be involved in many developmental and physiological processes, as well as in response to various stresses such as temperature and pathogen, etc. (Augustine and Vierstra, 2018; Castro et al., 2012; Miura and Hasegawa, 2010). Consequently, SIZ1 has more than 1000 described targets (Rytz et al., 2018), and its mutants display pleiotropic phenotypes including dwarfism of adult plants (Lee et al., 2007; Saracco et al., 2007). During heat shock SIZ1 is the main driver of sumoylation where it uses SUMO1 and SUMO2 as substrates (Saracco et al., 2007).

SIZ1 also sumoylates several transcription factors (Garcia-Dominguez et al., 2008; Liu et al., 2019; Miura et al., 2005, 2007, 2009; Zhang et al., 2020; Zheng et al., 2012) with contrasting effects, depending on the substrate. For example, sumoylation of ABI5 negatively regulates abscisic acid signalling (Miura et al., 2009), whereas sumoylation of ICE1 has a positive effect on cold tolerance (Miura et al., 2007). SIZ1 is therefore a major regulator of transcription in Arabidopsis, although it is not specific to any signalling pathway or family of substrate proteins.

To date, STOP1 has not been reported in any proteomic analysis of SIZ1-dependent sumoylated proteins of Arabidopsis (Rytz et al., 2018), and a functional link between SIZ1 and STOP1 was established only very recently (Fang et al., 2021a; Xu et al., 2021). In this work, we genetically identified the SUMO ligase SIZ1 as a modulator of STOP1 activity that decreases the abundance of the STOP1 protein in the root tip. These results demonstrate a role for SIZ1 in STOP1 signalling.

RESULTS

KO mutations of SIZ1 partially suppress a leaky mutation of stop1

To identify genes involved in the STOP1 signalling pathway, we devised a suppressor screen of a *stop1* mutant. Because we aimed to target STOP1-dependent suppressors, we chose to perform the mutagenesis on a leaky *stop1* mutant (*stop1^{33}*). The *stop1^{33}* mutant is characterized by a recessive missense mutation (P167L) and was isolated during an ethyl methane sulphonate mutagenesis screen (Balzergue et al., 2017). The sensitive *pALMT1::GUS* reporter of STOP1 activity (Balzergue et al., 2017) was

introgressed into a *stop1³³* background. The reporter construct showed that seedlings homozygous for *stop1³³* harbour a low, residual STOP1 activity (see below).

We performed a fast neutron (FN) mutagenesis as previously described (Belfield et al., 2012) on several thousand *stop1³³*; *pALMT1::GUS* seeds (see Experimental Procedures for details). The irradiated seeds were then sowed on soil in order to obtain the M2 generation of seeds. To isolate suppressors of *stop1³³*, we elaborated a forward genetics screen composed of three successive steps aimed at enhancing the specificity of the screen toward STOP1-dependent signalling. These three steps rely on the role of STOP1 in two growth conditions that inhibit root elongation.

Briefly (see Experimental Procedures for details), M2 seedlings were first grown in medium with a toxic level of Al^{3+}. Under this growth condition, parental *stop1³³* seedlings grow poorly (i.e. very short primary root), whereas WT seedlings have a long primary root. We thus selected mutants with a long primary root, and the progeny of these individual plants were then grown on −Pi plates to identify plants in which the primary root is more sensitive to the −Pi medium (i.e. shorter root than the parental line). Then, in the third step, among the lines that passed the first two steps, we selected those that displayed a higher expression of *ALMT1* in the root tip under −Pi, as assessed by the *pALMT1::GUS* marker. Forty suppressors were isolated out of ~450 000 M2 seeds used in the first step.

This work focuses on two of these mutants, *sup33-46* and *sup33-90*, which display similar stunted growth phenotypes in the adult stage (Figure S1). The two mutants were backcrossed with the parental *stop1³³* line, and the F2 of this backcrossed population was analysed for segregation of primary root length under −Pi (Figure S2). From these data, we estimated that there were approximately 22% (of 419 individuals) and 21% (of 276 individuals) in the F2 with a root length as long as in the corresponding *sup33-46* and *sup33-90* single mutants. This is lower than the expected 25% ratio for a recessive mutation, and it is likely that the translocated chromosome arms (see below) biased the segregation.

To identify the causal mutations in the two mutants, we analysed results from deep sequencing of genomic DNA. Briefly (see Experimental Procedures for details), for each mutant line, several homozygous plants were selected in the F2 of a backcross, from which we made a pooled DNA extraction. A library was then made, and DNA was sequenced by paired ends. The reads were then analysed for the presence of mutations.

A translocation that alters the *SIZ1* gene (AT5G60410) was identified in each of the two suppressors (Figure 2). In *sup33-46*, the 5′-part of *SIZ1* is joined to the 3′-part of At5g49110 (a gene with no known function). In *sup33-90*, the 5′-part of the *SIZ1* gene is joined to the 5′-part of At2g27430 (a gene coding an ARM repeat superfamily protein with no known function). These translocations detected by deep sequencing were confirmed by polymerase chain reaction (PCR) on independent DNA extractions (Figure S3). Because the *sup33* homozygous mutants are viable, the translocated arms carrying the distal part of *SIZ1* are still present in the mutant genomes, possibly as balanced translocations. However, we did not characterize them.

As the *sup33-46* and *sup33-90* independent mutations are predicted to truncate more than three-quarters of the SIZ1 protein, we believe these alleles are very strong, if not null. In order to confirm that mutations of the *SIZ1* gene are the causative suppressor mutations we used a third allele, *siz1-3* (in a Col-0 background), whose mutation is caused by a T-DNA inserted inside *SIZ1* (Miura et al., 2005; Figure S4). Note that the adult *siz1-3* mutant displays the same adult phenotype as our two suppressors (Figure S1).

We first examined the null hypothesis that *siz1* mutations are not suppressors of *stop1³³*. F2 seeds from a cross between *stop1³³* and *siz1-3* were sown on a −Pi plate, and seedlings with a typical Stop1³³ phenotype (i.e. a long primary root) were transferred to soil to obtain adult plants. If the *siz1-3* mutation is not a suppressor of *stop1³³*, we would expect to obtain about one-quarter of plants with a Siz1⁻ phenotype. As shown in Figure S5a, we did not observe any such phenotype among the 24 cultivated plants. We then PCR-genotyped these plants for the presence or absence of the *siz1-3* mutation, and identified 11 heterozygous and 13 WT plants. No *siz1-3* homozygous plants were observed (Figure S6), therefore confirming the visual inspection of the plants. We thus rejected the null hypothesis that the *siz1-3* mutation is not a suppressor of *stop1³³*.

In parallel, we performed the same test with the *stop1¹²⁷* null allele (Balzergue et al., 2017) crossed with *siz1-3*: among 24 F2 plants we obtained six plants with a rosette morphology typical of the *siz1-3* mutant (Figure S5b). This 1:4 ratio is expected for the segregation of a recessive mutation that does not interfere with the expression of the Stop1¹²⁷ phenotype. In this case, we accepted the null hypothesis that *siz1-3* is not a suppressor of *stop1¹²⁷*. Finally, different combinations of crosses between the suppressor lines with *stop1³³;siz1-3*, *siz1-3* and *stop1³³* confirmed that mutations in *SIZ1* suppress *stop1³³* in *sup33-46* and *sup33-90* (Figure S7).

Taken together, these results demonstrate that *siz1-3* is a recessive suppressor of *stop1³³*. They also indicate that *siz1-3* cannot suppress the *stop1* null allele. We thus conclude that the *siz1* mutations in the *sup33-46* and *sup33-90* mutants cause the suppressor phenotypes in the *stop1³³* background.
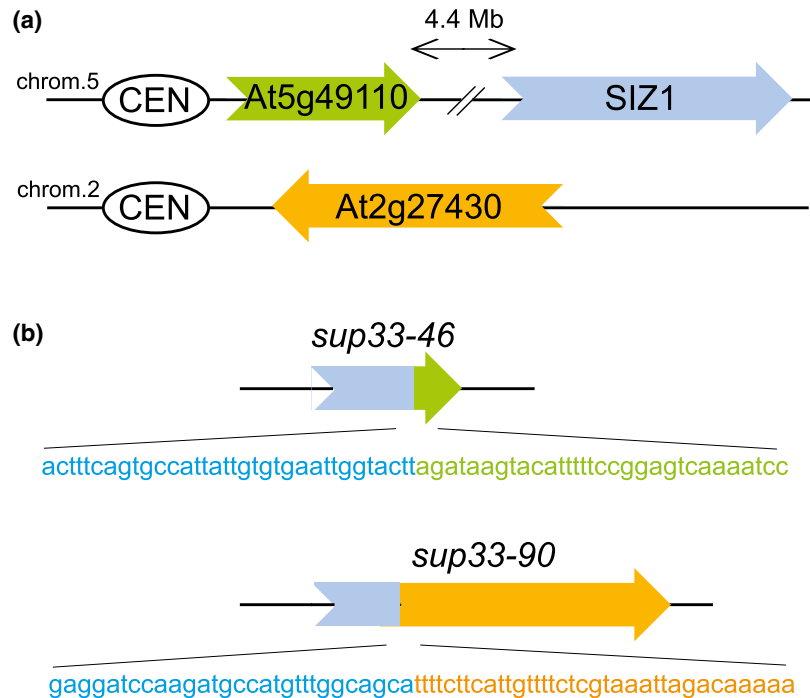
(a)

4.4 Mb

chrom.5 CEN At5g49110 SIZ1

chrom.2 CEN At2g27430

(b)

sup33-46

actttcagtgccattattgtgtgaattggtactt agataagtacatttttccggagtcaaaatcc

sup33-90

gaggatccaagatgccatgtttggcagca ttttcttcattgtttttctcgtaaattagacaaaaa

Figure 2. Schematic of the structure of translocations that alter the *SIZ1* gene in the *sup33-46* and *sup33-90* mutants.
(a) Genomic structure in the wild-type (WT).
(b) Genomic structure of the *siz1* gene in the *sup33* mutants.
Centromeres (CEN) are indicated relative to the genes. Genes are symbolized as coloured arrows, with arrowheads indicating the direction of transcription. Symbols are not to scale. The DNA sequence (from NGS) at the translocation junction is given for each mutation [see Figure S3 for the polymerase chain reaction (PCR) confirmation of the mutations]. For each mutant, only the 5′-moiety of *siz1* is shown.

To further characterize the suppressor phenotype, we generated a *siz1-3; stop1[33]; pALMT1::GUS* triple homozygous line. We measured primary root growth and assessed *ALMT1* expression in seedlings grown under conditions where STOP1 is activated (namely in the presence of Al^{3+} or under −Pi). In the absence of Al^{3+}, the primary roots of all examined mutants grow like the WT (Figure 3a). By contrast, in growth medium containing 30 μM Al^{3+}, longer primary roots were observed in *sup33-46*, *sup33-90* and the double mutant *siz1-3; stop1[33]* than in the *stop1[33]* single mutant (Figure 3a; see also Figure S8 for a duplicate experiment). The enhanced root resistance to Al^{3+} is mirrored by the expression level of *ALMT1* in the root tip, as visualized with the *pALMT1::GUS* marker (Figure 3b). Indeed, compared with the WT, the *stop1[33]* single mutant poorly expresses *ALMT1*, whereas the two *sup33* mutants and the *siz1-3; stop1[33]* double mutant have a stronger expression than the *stop1[33]* single mutant. These results confirm that *SIZ1* loss-of-function mutations enhance the resistance of primary roots to growing in the presence of Al^{3+}, and this is correlated with the expression level of *ALMT1*.

Compared with the Al^{3+} stress, STOP1 and ALMT1 have an opposite effect on primary root growth under the −Pi condition. Figure 3a shows that under the −Pi condition, *sup33-46*, *sup33-90* and the double mutant *siz1-3; stop1[33]*

have shorter primary roots than the *stop1[33]* single mutant (see also Figure S9 for a duplicate experiment). The suppression effect of *siz1* mutations on the Stop1[33] root phenotype is correlated with a stronger *ALMT1* expression in the root tip as compared with *stop1[33]* (Figure 4b).

Therefore, in both Al^{3+} and −Pi stress conditions, the suppression effect of *siz1* mutations is correlated with higher expression of *ALMT1*. Note that in both conditions, and for the two observed phenotypes (primary root length and intensity of GUS staining), none of the three *siz1* mutations completely restored *stop1[33]* primary root length or *AMLT1* expression to WT levels. We thus conclude that the suppression is incomplete or partial. Altogether, these genetic results confirm that the KO mutation of *SIZ1* partially suppresses the leaky *stop1[33]* mutation.

The suppression phenotype depends on STOP1 activity

Our result with the segregating population of rosette plants indicates that *siz1-3* does not suppress the *stop1[127]* null allele (Figure S5b). In order to further strengthen this preliminary conclusion, we created the *siz1-3; stop1[127]; pALMT1::GUS* triple homozygous mutant, and the seedlings were grown under both Al^{3+} and −Pi conditions.

No detectable GUS staining was found in the root tip of the *stop1[127]* single mutant in any of the tested growth
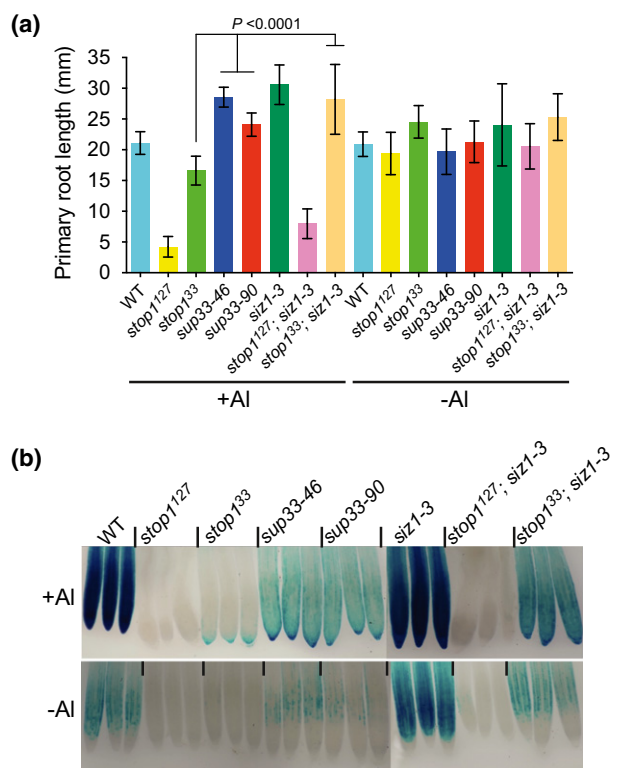
(a)

(b)

Figure 3. Primary root length and GUS staining of seedlings grown with or without Al^{3+}.

(a) Primary root length. Three-day-old seedlings were transferred for 3 days to medium with or without 30 μM Al^{3+} before measuring the primary root length. Mean ± SD, n = 15–27 seedlings per line and condition. Student's t-test was performed between the parental $stop1^{33}$ line and the $stop1^{33};siz1$ double mutants. See Figure S8 for a duplicate experiment.

(b) Images of GUS staining of the primary root tip from representative seedlings grown in (a). All lines are homozygous for the same *pALMT1::GUS* marker.

(a)

(b)

Figure 4. Primary root length and GUS staining of seedlings grown under –Pi.

(a) Primary root length. Three-day-old seedlings were transferred for 3 days to a –Pi medium with or without 10 μM Fe^{2+} before measuring the primary root length. Mean ± SD, n = 16–29 seedlings per line and condition. Student's t-test was performed between the parental $stop1^{33}$ line and the $stop1^{33};siz1$ double mutants. See Figure S9 for a duplicate experiment.

(b) Images of GUS staining of the primary root tip from representative seedlings grown in (a). All lines are homozygous for the same *pALMT1::GUS* marker.

conditions (Figures 2b and 3b). This confirms that STOP1 is required for the expression of *ALMT1* (Balzergue et al., 2017; Iuchi et al., 2007).

Under both the Al^{3+} and –Pi conditions, the primary root growth of the $siz1-3$; $stop1^{127}$ double mutant was similar to that of the $stop1^{127}$ single mutant (Figures 2, 3, Figures S8 and S9); furthermore, there was no detectable GUS staining in the root tip, as in the $stop1^{127}$ single mutant (Figures 2b and 3b). The $stop1^{127}$ mutation is therefore epistatic over $siz1-3$ for the expression of *ALMT1* and primary root growth. These results confirm that $siz1-3$ does not suppress the phenotype of the $stop1^{127}$ mutant. We therefore conclude that the suppression phenotype seen with $stop1^{33}$ depends on the residual activity of its mutant stop1 protein. These results demonstrate that SIZ1 is a modulator of the STOP1 signalling pathway.
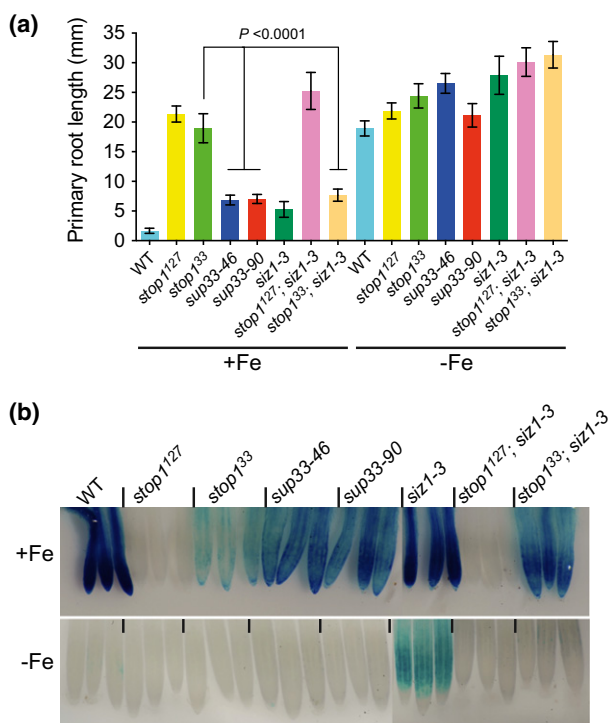
Test of STOP1 sumoylation in *Escherichia coli*

We hypothesized that SIZ1 could directly sumoylate the STOP1 protein using the core sumoylation machinery.

Biochemical detection of sumoylation *in planta* can be very challenging. Indeed, it has been reported that only a small fraction of the pool of a given substrate protein is sumoylated at any time (Augustine and Vierstra, 2018). This detection problem is exacerbated when focussing on a minuscule tissue like the Arabidopsis root tip where the protein of interest is also poorly expressed. To circumvent this problem, we used *E. coli* as a recipient system in which we expressed the Arabidopsis sumoylation machinery (Okada et al., 2009).

First, we checked whether we could detect sumoylation with this system. For this, we expressed the core machinery of sumoylation (SAE1, SAE2, SCE1) and His-tagged SUMO1 in *E. coli* (Figure S10). As shown in Figure 5a, after IPTG-induction of these four recombinant proteins, a

number of bands were visible with the anti-His antibody, many of which are likely to be sumoylated proteins of *E. coli* (compare lanes 1 and 2 in Figure 5a; see Figure S10 for loading controls). We further validated this sumoylation system using the Arabidopsis transcription factor MYB30 as a positive control (Okada et al., 2009). Sumoylation of a tested protein can be observed by the appearance of high-molecular-weight forms. When His-MYB30 was co-expressed with the sumoylation machinery, we detected an additional band of 55 kDa, corresponding to His-MYB30 tagged with His-SUMO1, as previously observed (Okada et al., 2009; compare lane 6, red arrowhead, with lanes 2 and 4 in Figure 5a). A second experiment, where we treated the samples with a SUMO protease to remove the SUMO1 tag, was conducted to confirm that the new band was a genuine mono-sumoylated form of MYB30. We therefore produced the *Saccharomyces cerevisiae* SUMO protease ScUlp1 by expression in *E. coli* (Figure S12). ScUlp1 shares high sequence similarity with the Arabidopsis SUMO protease AtUlp1, especially in catalytic residues and residues in direct contact with the SUMO substrate (Mossessova and Lima, 2000). When protein extracts from *E. coli* expressing the sumoylation machinery were treated with the yeast SUMO protease before performing sodium dodecyl sulphate–polyacrylamide gel electrophoresis (SDS–PAGE), most of the His-signals disappeared (compare lanes 2 and 3 in Figure 5b; see Figure S11b for loading controls). Furthermore, the SUMO protease eliminated the band corresponding to mono-sumoylated MYB30 (compare lanes 4 and 5 in Figure 5b).

After validating the reconstituted sumoylation assay, we tested the sumoylation of STOP1 using the core sumoylation complex, initially in the absence of SIZ1. Indeed, some substrates do not require the E3 SUMO ligase SIZ1 for sumoylation when using an *in vitro* reconstituted system or *E. coli* (Elrouby and Coupland, 2010; Liu et al., 2019; Mazur et al., 2017; Zhang et al., 2019a), while other substrates do (Kim et al., 2015a,b; Miura et al., 2007; Zhang et al., 2020).

The coding sequence of the full-length Arabidopsis *SIZ1*, with codons optimized for expression in *E. coli* (Figure S14), was well expressed in *E. coli* (Figure S15). The anti-HA immunoblot was able to detect the HA-STOP1 protein (expected at 59.3 kDa, but observed at about 70 kDa) when expressed alone (see lane 2 in Figure 6a; see Figure S13 for loading controls). However, when the core sumoylation machinery was co-expressed with HA-tagged STOP1, the anti-HA did not reveal any high-molecular-weight HA-STOP1 proteins (see lane 4 in Figure 6a). In addition, a similar blot hybridized with the anti-His antibody (to detect His-SUMO1) did not reveal any new bands (compare lanes 4 and 5 in Figure 6b), suggesting that in addition to the core sumoylation machinery, SIZ1 might be necessary for the efficient sumoylation of STOP1.

To further examine this hypothesis, we co-expressed SIZ1 with the core sumoylation machinery, which notably changed the pattern of the anti-His immunoblot (compare lanes 1 and 5 in Figure 6b). As previously found with this assay, SIZ1 was functional in *E. coli* (Okada et al., 2009).

In contrast, co-expressing SIZ1 and the core sumoylation machinery with STOP1 did not reveal any new, high-molecular-weight forms of STOP1 (see lane 3 in Figure 6a), although, for some unknown reason, it is more abundant than when SIZ1 is not co-expressed (compare lanes 3 and 4 in Figure 6a; see Figure S13 for the loading control). Thus, although the Arabidopsis core sumoylation machinery and SIZ1 were active, we did not detect any sumoylated STOP1 in *E. coli*.

Al^{3+} and mutation in *SIZ1* additively increase the accumulation of STOP1

Next, we tested whether mutation of *SIZ1* alters STOP1 abundance in roots. The *pSTOP1::GFP-STOP1* construction (Balzergue et al., 2017) was introduced by crossing into a *siz1^{GK}* mutant background. Four-day-old seedlings were transferred on a medium with or without Al^{3+} for 4 h, and proteins were then extracted from root tips for Western blot analysis. Using an antibody against GFP, we detected a signal at the expected size (82.2 kDa) for the GFP-STOP1 fusion protein (Figure 7a). We then quantified the signal relative to the GAPC loading control obtained on the same membrane (Figure 7b). This confirmed our previous results, namely that Al^{3+} stimulates the accumulation of GFP-STOP1 in WT root tips (Godon et al., 2019). Interestingly, in the *siz1* mutant not treated with Al^{3+} the GFP-STOP1 protein was slightly more abundant than in the WT, and this accumulation was exacerbated by Al^{3+} treatment, revealing an additive effect involving Al^{3+} and the *siz1* mutation.

Compared with the WT, the higher abundance of STOP1 in the *siz1* single mutant is mirrored by the higher expression of *ALMT1* in the root tip. This is particularly visible under the −Al (Figure 3b) and −Fe (Figure 4b) conditions, where *ALMT1* is poorly expressed in the WT. Taken together, these results suggest that the partial suppression of the Stop1[33] phenotype in *siz1* backgrounds results from the increased abundance of the mutant stop1[33] protein.

DISCUSSION

Previous work has reported that STOP1 is sumoylated *in vivo* and *in vitro* by SUMO1, and that the SUMO protease ESD4 desumoylates SUMO1-tagged STOP1 (Fang et al., 2020). The authors also identified three lysine residues that, when substituted by arginine, alter sumoylation and the stability and activity of STOP1. Sumoylation of STOP1 is therefore a way to regulate its stability and activity. They subsequently showed that in protoplasts of the *siz1* mutant, recombinant STOP1 is much less sumoylated
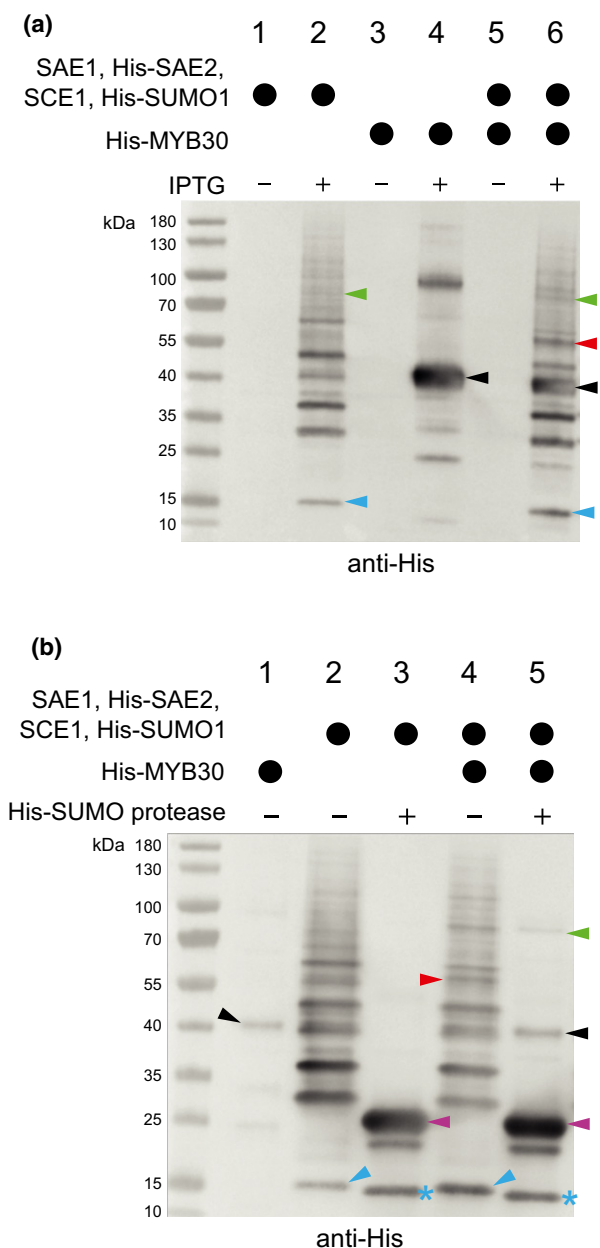
(a)

(b)

Figure 5. Sumoylation of AtMYB30 by the reconstituted Arabidopsis sumoylation complex in *Escherichia coli*.

(a) *E. coli* BL21 (DE3) cells were transformed with plasmids expressing the proteins of the Arabidopsis core sumoylation complex and/or His-MYB30 as indicated by the schematic. Transformed *E. coli* strains were incubated at 37°C until the OD_{600} reached 0.6–0.7. Next, IPTG was added (+) or not (−) to the cultures to induce the expression of recombinant proteins, and cultures were incubated overnight at 25°C. Cell extract aliquots equivalent to 30 μg of proteins were then loaded in each lane and a Western blot was performed with an anti-His-tag antibody. When expressed alone, His-MYB30 was detected at its expected molecular weight (38.9 kDa; black arrowhead; 4th lane). When His-MYB30 was co-expressed with the sumoylation complex, a new band with a molecular weight corresponding to a mono-sumoylated form of His-MYB30 (50.9 kDa expected, 55 kDa observed) was detected (red arrowhead) in addition to the native form of His-MYB30 (black arrowhead; 6th lane). Green arrowheads: His-SAE2; blue arrowheads: His-SUMO1.

(b) SUMO protease assay. Expression in *E. coli* of the indicated proteins was IPTG-induced [as in (a)], and all cell lysates were incubated overnight at room temperature under gentle agitation with (+) or without (−) a purified His-tagged SUMO protease (Figure S12). After sodium dodecyl sulphate–polyacrylamide gel electrophoresis (SDS–PAGE), a Western blot was performed with an anti-His antibody. See Figure S11 for gel loading controls. Treatment with the SUMO protease cleared the immunoblot, including the signal corresponding to the mono-sumoylated His-MYB30. Black arrowheads: His-MYB30; red arrowhead: mono-sumoylated His-MYB30; blue star: SUMO1 presumably linked to a bacterial peptide or small bacterial protein; purple arrowheads: His-tagged SUMO protease. See Figure S11 for the gel loading controls.

than in the WT. In a similar assay, Xu et al. also observed the reduced sumoylation of STOP1 (Xu et al., 2021).

In this study, we used forward genetics to identify SIZ1 as a novel gene that regulates the STOP1 signalling pathway. We isolated two *siz1* mutations using the leaky *stop1³³* mutant as a parental line for the mutagenesis, combined with a three-step phenotypic screen. Our results confirm that *siz1* is the causal suppressor mutation with a third allele, *siz1-3*, introgressed in the *stop1³³* background. While all three *siz1* mutations are strong alleles, they only partially suppress the sensitivity of *stop1³³* seedlings to Al^{3+} and their insensitivity to −Pi. Importantly, we demonstrate that the suppression mechanism of *siz1* mutations

depends on STOP1 activity: in a *stop1* null background, there is no suppression of the typical Stop1⁻ growth phenotypes, and expression of *ALMT1* is not restored. We therefore conclude that *siz1* requires STOP1 activity to exert its suppressor effect on STOP1 signalling. Altogether, our genetics data show that SIZ1 negatively modulates the STOP1 signalling pathway triggered by Al^{3+} and Fe^{2+}.

One suppressor screen of *stop1* has been reported in the literature, but with a different goal from our study, as the authors used a *stop1* null allele as a parental line for the mutagenesis (Jiang et al., 2017). The authors therefore isolated mutations whose suppression mechanism is at least partially STOP1-independent. Furthermore, SIZ1 was not identified in the linkage areas of the mutants that they mapped.

We strongly believe that the role of SIZ1 in primary root growth inhibition under −Pi is not mediated through sumoylation of the transcription factor PHR1 (Miura et al., 2005), a master regulator of Pi homeostasis, as we previously showed that PHR1, as well as PHF1 (PHOSPHATE TRANSPORTER TRAFFIC FACILITATOR 1) regulating Pi transporters, are not involved in this STOP1-dependent response to −Pi (Balzergue et al., 2017; Thibaud et al., 2010). SIZ1 is therefore a strong candidate for the E3 ligase that directly sumoylates STOP1 under Al and −Pi stresses. Other work has shown that STOP1 is ubiquitinated by the ubiquitin ligase RAE1 and that this ubiquitination decreases STOP1 abundance via proteasomal degradation (Zhang et al., 2019b).
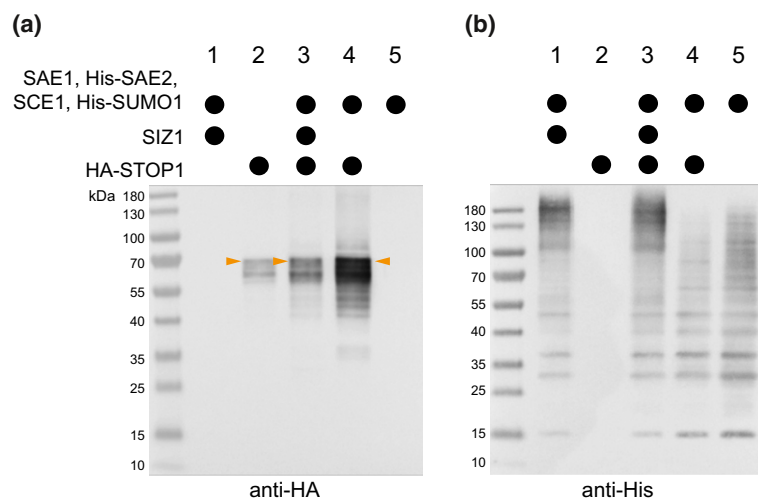
(a)

(b)

Figure 6. STOP1 sumoylation assay using the reconstituted sumoylation complex and SIZ1 in *Escherichia coli*.
Escherichia.coli BL21 (DE3) cells were transformed with plasmids expressing various proteins as indicated in the schematic. Transformed *E. coli* strains were incubated at 37°C until the OD_{600} reached 0.6–0.7. Next, IPTG was added to the cultures to induce the expression of recombinant proteins, and cultures were incubated overnight at 25°C. Cell extract aliquots equivalent to 30 μg of proteins were then loaded in each lane and Western blots were performed with an anti-HA-tag (a) or an anti-His-tag (b) antibody. HA-STOP1 was detected (orange arrowheads) (a), but no sumoylated form was detectable (a, b). See Figure S13 for gel loading controls.

It is tempting to hypothesize that sumoylation of STOP1 is a signal for its subsequent ubiquitination and consequent degradation. We therefore tested the hypothesis that SIZ1 can directly sumoylate STOP1 using an *E. coli*-based sumoylation assay. This was first performed using the Arabidopsis core sumoylation machinery alone, which is known to be sufficient in certain cases for sumoylation *in vitro* or in *E. coli*, and then by adding SIZ1. However, although we verified that the Arabidopsis sumoylation complex proteins were produced and functional in *E. coli* (on *E. coli* proteins and on Arabidopsis MYB30), we did not detect any sumoylated forms of STOP1, either with the core machinery alone or after adding SIZ1. Intriguingly, after this study was submitted, an article reporting sumoylated forms of STOP1 using a similar *E. coli*-based sumoylation assay was published (Xu et al., 2021). These sumoylated forms of STOP1 were observed with the Arabidopsis core sumoylation machinery and without co-expressing SIZ1. However, several controls necessary to firmly conclude that STOP1 is sumoylated in this *E. coli* assay were not shown, including a sumoylation test without STOP1 as a negative control and a Coomassie-stained gel showing the nickel-sepharose purification steps used to purify the sumoylated His-tagged STOP1 proteins. Furthermore, it would have been interesting to express SIZ1 with the core sumoylation machinery in this assay to determine if SIZ1 can improve the efficiency of STOP1 sumoylation. Determining whether STOP1 is sumoylated in *E. coli* and whether SIZ1 participates in this reaction will therefore require further study.

Several reasons could explain why we did not detect any sumoylated forms of STOP1 in *E. coli*. Sumoylation of STOP1 may depend on a prior post-translational modification that does not occur when it is expressed in *E. coli*. For example, phosphorylation and sumoylation could act interdependently to modulate stress responses (Tomanov et al., 2018; Vu et al., 2018). Moreover, there are several reported cases in animal cells of phosphorylation-dependent SUMO modifications of the substrate (Hietakangas et al., 2006).

One recent phosphoproteome study of Arabidopsis identified two STOP1 phosphorylation sites in cell culture extracts (Mergner et al., 2020). However, the phosphorylated amino acid residues (S25 and S79) are not close to any of the three sumoylated lysines identified in STOP1 (K40, K212 and K395; Fang et al., 2020), and no STOP1 phosphopeptides were detected in the roots. Indeed, there is currently no evidence supporting the idea that STOP1 is phosphorylated in the roots, especially under conditions that modulate its stability such as pH, Al^{3+} and $-Pi$ stress.

Another possibility to explain the absence of STOP1 sumoylation in *E. coli* is that sumoylation of STOP1 may require a protein partner (or that STOP1 needs to be included in a multiprotein complex). One model for E3 ligase activity in animal cells is of a cooperative system in which sumoylation of several subunits within a protein complex occurs after binding of the E3 ligase to a single subunit (the 'SUMO spray' model; Augustine and Vierstra, 2018). One such complex, the conserved Mediator complex, participates in transcriptional activation/repression, and several of its subunits are reportedly sumoylated in Arabidopsis (Augustine and Vierstra, 2018). It is possible that when SIZ1 modifies the Mediator complex, it might
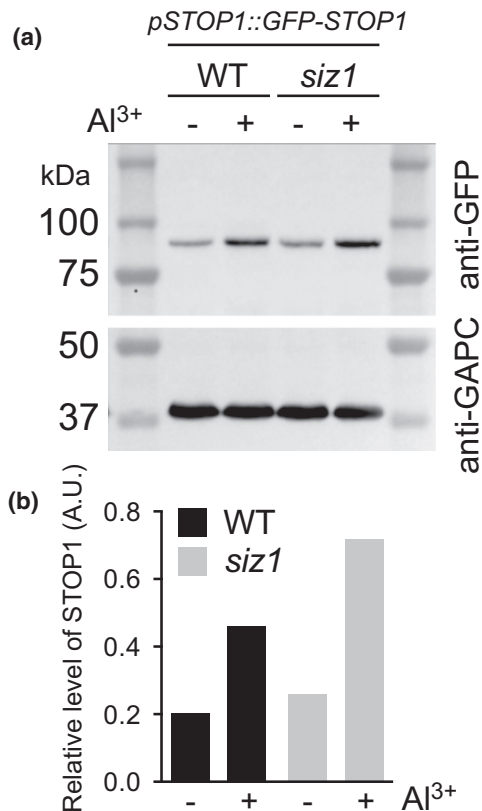
(a)

pSTOP1::GFP-STOP1

WT   *siz1*

Al^{3+} -   +   -   +

(b)

Figure 7. Additive effect of Al^{3+} and the *siz1* mutation in the accumulation of GFP-STOP1 in the root tip.
(a) GFP-STOP1 abundance in root tips. Four-day-old seedlings carrying the same *pSTOP1::GFP-STOP1* construct were transferred for 4 h on a medium with (+) or without (−) 100 μM Al^{3+}, and proteins were extracted for Western blotting using anti-GFP antibody (top). Uncropped images are provided in Figure S16. The blot was rehybridized with an anti-GAPC antibody as a loading control (bottom).
(b) Quantification of GFP-STOP1 abundance in wild-type (WT) and *siz1*. The level of GFP abundance was quantified relative to the corresponding GAPC level.

also sumoylate STOP1. Interestingly, MED16, a protein in the Mediator complex, physically interacts with STOP1 (Raya-González et al., 2020). MED16 has a positive role in the transcription of STOP1 targets, and *med16* mutant seedlings have a Stop1$^-$-like phenotype under both −Pi (Raya-González et al., 2020) and Al^{3+} (Xu et al., 2021). This growth phenotype is opposite to that of *siz1*, perhaps because the putative role of MED16 in the sumoylation of STOP1 is epistatically masked by its more crucial transcriptional functions. Interestingly, using Arabidopsis protoplasts, Xu et al. observed that the combined K40R and K212R mutations in STOP1 increase the level of MED16 co-immunoprecipitated, although this effect seems rather modest (Xu et al., 2021). This suggests that sumoylation of STOP1 inhibits interaction with MED16, perhaps to inhibit STOP1 transcriptional activity.

Our results show that the root tips of *siz1* mutants accumulate more STOP1 protein than in the WT (Figure 7). This result is in contrast to other recent studies (Fang et al., 2021a; Xu et al., 2021), especially under Al^{3+} stress. This discrepancy could be due to different experimental protocols, as Fang et al. (and probably also Xu et al.) used proteins extracted from whole roots (Fang et al., 2021a), whereas we used proteins from the root tip. By performing quantitative reverse transcriptase (qRT)-PCR on whole roots, Fang et al. and Xu et al. found that *ALMT1* is more highly expressed in the *siz1* mutant than in the WT (Fang et al., 2021b). Similarly, we found with the *pALMT1::GUS* reporter that the *siz1* mutation (in the leaky *stop1^{33}* background) enhances the expression of *ALMT1* in root tips (Figures 2 and 3). Thus, in these three works, the enhanced expression of *ALMT1* in *siz1* mutants correlates with an enhanced resistance to Al^{3+} and an enhanced response to Fe^{2+} (under −Pi).

Moreover, as Xu et al. (2021) have shown, we demonstrate that these phenotypes are STOP1-dependent (Figures 2 and 3). In addition, Xu et al. convincingly showed the epistasis of the *almt1* mutation over *siz1* for the exudation of malate and the root growth response to Al^{3+}. All these observations are in agreement with the fact that the sumoylation activity of SIZ1 downmodulates STOP1 signalling.

This is in sharp contrast to the results published by Fang et al. showing a positive correlation between similar responses and the level of STOP1 sumoylation (Fang et al., 2020). Indeed, the authors showed that mutations in the desumoylase ESD4 increase the sumoylation of STOP1 and the expression of *ALMT1* in roots, thus increasing the resistance against Al^{3+}. In addition, they report that Al stress reduces the level of STOP1 sumoylation in Arabidopsis plants. However, in contrast to *siz1*, the *esd4* mutations do not alter the abundance of STOP1 in roots.

How can these seemingly disparate observations be reconciled? First, using the transient expression of recombinant STOP1 and SUMO1 in protoplasts, Xu et al. and Fang et al. both observed reduced levels of sumoylation of STOP1 in the *siz1-2* mutant as compared with the WT (Fang et al., 2021a; Xu et al., 2021). SIZ1 therefore appears to participate in STOP1 sumoylation in plant cells. It is unclear if it participates directly, however, as we did not detect the sumoylated form of STOP1 in our reconstituted sumoylation assay in *E. coli* and Xu et al. did not test for SIZ1 in a similar assay (Xu et al., 2021). Nevertheless, using a combination of split luciferase and bimolecular fluorescence complementation assays in *Nicotiana benthamiana*, yeast two-hybrid assays, pull-down assays with bacterial extracts and co-immunoprecipitation from Arabidopsis protoplasts, Xu et al. and Fang et al. concluded that there is a physical interaction between STOP1 and SIZ1 (Fang et al., 2021a; Xu et al., 2021). These results

support the hypothesis that STOP1 is a target of SIZ1. It is therefore necessary to understand how sumoylation of STOP1 by SIZ1 and its desumoylation by ESD4 result in similar molecular and physiological responses.

Treatments with inhibitors of the 26S proteasome and of protein synthesis show that the steady-state level of STOP1 abundance results from a balance between synthesis and degradation, and that Al^{3+} stress reduces STOP1 degradation (Fang et al., 2020; Zhang et al., 2019b). In this dynamic turnover, cycles of sumoylation and desumoylation might be involved in such a manner that the deregulated sumoylation of STOP1 (e.g. as in the *siz1* and *esd4* mutants) alters the pool of active STOP1. A partially sumoylated state of STOP1 could be a condition for its proteasomal degradation.

Using site-directed mutagenesis, Fang et al. found three sumoylable lysines (K40, K212 and K395) in STOP1 (Fang et al., 2020), whereas Xu et al. only found the first two of this trio (Xu et al., 2021). The results of Fang et al. indicate that the K395R mutation partially destabilizes STOP1, whereas the single K40R and K212R mutations have little to no effect on its stability (Fang et al., 2020). However, any combination involving two of these mutations, or the three mutations together, partially destabilizes STOP1. It thus appears that some sumoylated states of STOP1 are more prone to destabilization than others. Alternative explanations for this conundrum probably exist and will require further investigation.

In conclusion, although we did not detect the sumoylated form of STOP1 in the presence of the Arabidopsis core sumoylation complex or SIZ1 in *E. coli*, our genetics results clearly demonstrate that the E3 sumo ligase SIZ1 is a regulator of STOP1-dependent *ALMT1* expression triggered by Al^{3+} and Fe signals.

EXPERIMENTAL PROCEDURES

Plant material

The Arabidopsis leaky allele *stop1*[33] and the null allele *stop1*[127] are both in a Col[er105] genetic background and come from an ethyl methane sulphonate mutagenesis screen (Balzergue et al., 2017). They were backcrossed twice to the Col[er105] parental line. Introgression was performed by crossing the *pALMT1::GUS* marker (*GUS, uidA* gene encoding β-glucuronidase; Godon et al., 2019) in the *stop1*[33] and *stop1*[127] mutant backgrounds to generate the double homozygous *stop1*[33]; *pALMT1::GUS* and *stop1*[127]; *pALMT1::GUS* lines.

Because the creation of lines combining several loci is hampered by translocations, most of our analyses were conducted with the *siz1-3* allele (SALK _034008). To create the *siz1-3*; *stop1*[33]; *pALMT1::GUS* triple homozygous line, we crossed a *stop1*[33]; *pALMT1::GUS* plant with pollen of *siz1-3*. In the F2 generation, 24 seedlings displaying a typical Stop1[33] phenotype under −Pi were selected and transferred to soil. None of the plants harboured the typical stunted phenotype of *siz1-3*. All plants were genotyped in order to identify those heterozygous for *siz1-3*. In the F3

generation, we selected a plant with a Siz1-3 phenotype that was also homozygous for phosphinothricin (PPT) resistance (the PPT resistance gene is on the T-DNA carrying the *pALMT1::GUS* marker) as a *siz1-3*; *stop1*[33]; *pALMT1::GUS* triple homozygous line. We followed the same procedure to create the *siz1-3*; *stop1*[127]; *pALMT1::GUS* triple homozygous line, except that in the F2 there were several plants homozygous for *siz1-3*. The *pSTOP1::GFP-STOP1* marker (Balzergue et al., 2017) was introgressed in the *siz1*[GK] (GABI_217A09) mutant background by crossing.

Plant growth

Plants in soil were grown in long (16 h photoperiod) or short days (8 h photoperiod), at 22°C (day)/21°C (night).

Seedling growth

Seeds were surface-sterilized for 2 min in a solution containing 70% ethanol and 0.05% SDS, and were washed twice with 96% ethanol.

The nutrient solution contained 0.47 mM $MgSO_4$, 2.1 mM NH_4NO_3, 1.89 mM KNO_3, 0.67 mM $CaCl_2$, 0.5 μM KI, 0.79 μM H_3BO_3, 10 μM $MnSO_4$, 5 μM $ZnSO_4$, 1 μM $Na_2 MoO_4$, 0.1 μM $CuSO_4$, 0.1 μM $CoCl_2$ and 5 g L^{-1} sucrose. The agar (8 g L^{-1}) for plates was from Sigma-Aldrich (A7921 Lot BCBZ7284; see Table S1 for elemental composition). The −Pi and +Pi agar media, respectively, contained 0 and 500 μM KH_2PO_4, supplemented with 10 μM $FeCl_2$ and 5 μM $AlCl_3$; the media were buffered at pH 5.8 with 3.4 mM 2-(*N*-morpholino)ethanesulphonic acid (MES). The −Al media contained 500 μM KH_2PO_4, 10 μM $FeCl_2$ and no $AlCl_3$, while the +Al media contained 0 μM KH_2PO_4, 2 μM $FeCl_2$ and 30 μM $AlCl_3$. The medium was buffered at pH 5.5 with 3.4 mM MES.

For the root growth experiment, seeds were sown on +P medium. After 3 days, plantlets were transferred on either −P, +P, −Al or +Al medium for 3 days.

For Western blot analysis, seeds were sown side by side in a line on four strips (5 × 1.3 cm) of nylon mesh (SEFA03-5/1). Each mesh contained 70–80 seeds, therefore totalling 280–320 seedlings per sample. Meshes were then placed on a sterile growth medium to allow seedlings to grow. After 4 days, the meshes with seedlings were transferred to the fresh medium without $FeCl_2$, in the presence or absence of 100 μM $AlCl_3$. After 4 h, the root tips (about 1 cm, from the tip) were cut with a razor blade, harvested and frozen in liquid nitrogen.

Mutagenesis and suppressor screen

A batch of 1.666 g of seeds representing ~93 200 seeds (*stop1*[33]; *pALMT1::GUS*) were mutagenized by 60 Gy of FN (HAS Centre for Energy Research; Budapest, Hungary) and subsequently sown in soil; plants were then grown in a phytotron. An estimated 44 000 M1 plants were grouped in 152 pools from which M2 seeds were collected.

Each pool was screened following a three-step protocol. In the first step, ~25–30 mg of M2 seeds was surface-sterilized and sown in a 2-L flask containing 100 mL of growth medium (0.15 mM $MgSO_4$, 2.1 mM NH_4NO_3, 1.9 mM KNO_3, 0.34 mM $CaCl_2$, 0.5 μM KI, 10 μM $FeCl_2$, 10 μM H_3BO_3, 10 μM $MnSO_4$, 3 μM $ZnSO_4$, 0.1 μM $CuSO_4$, 0.1 μM $CoCl_2$, 0.1 μM $Na_2 MoO_4$, 200 μM $CaCl_2$, 5 g L^{-1} sucrose, 200 μM HomoPipes pH 4) with 14 μM Al^{3+}. Flasks were placed in a growth chamber (see above) and rotationally agitated (130–140 rpm). After 3 days, seedlings with a long primary root (presumably more resistant to this toxic medium) were transferred onto +Pi agar plates (see above) for recovery; several days

later they were transferred to soil in order to obtain the M3 progeny. Twenty–thirty M3 seeds from these selected M2 lines were then sown in −Pi plates (see above) in order to identify seedlings with a primary root shorter than that of the parental *stop1*[33] line (i.e. more sensitive to the −Pi condition). These M3 seedlings were then stained with X-gluc to assess the expression of *ALMT1* (*pALMT1::GUS*) in the primary root tip.

Lines showing a GUS staining significantly higher than in the parental line were kept for further analysis.

All of the pools were screened twice, representing a total of ∼450 000 screened M2 seeds, from which we selected 40 lines referred to as 'suppressor of *stop1*[33]' (abbreviated as *sup33*).

Mapping *sup33-46* and *sup33-90* mutations by NGS

Plant DNA extraction.   DNA was extracted in liquid nitrogen using a CTAB (cetyltrimethyl ammonium bromide) buffer (25% w/v) as previously described (Weigel and Glazebrook, 2002).

DNA deep sequencing.   In the F2 population of the backcross with the parental line, we selected 34 plants homozygous for the *sup33-46* mutation and 40 plants homozygous for the *sup33-90* mutation. Leaf material and extracted DNA were pooled from each mutant population. Respectively, 0.68 and 0.62 μg of DNA from the *sup33-46* and *sup33-90* pools were used to construct paired-end DNA libraries. DNA sequencing of paired-end reads (2 × 150 bp) was performed by GeT-PlaGe (https://get.genotoul.fr/la-plateforme/get-plage/) on an Illumina Hiseq 2000 platform.

Bioinformatics analyses were performed on the Genotoul Bioinformatics platform Toulouse Occitanie web server (https://vm-galaxy-prod.toulouse.inra.fr/galaxy).

Mapping reads.   Reads were first filtered using the 'Filter by quality' tool (version 1.0.0). PCR duplicate paired-end reads were removed using Rmdup (version 1.0.0). The remaining paired-end reads were mapped on the *Arabidopsis thaliana* TAIR 10 genome (https://www.arabidopsis.org) using BWA (Burrows-Wheeler Aligner; version 0.7.17.3). Reads were then filtered using Filter SAM (Sequence Alignment/Map; version 1.0.0). Only primary alignments of paired reads mapped in a proper pair were kept for further analysis. RealignerTargetCreator and IndelRealigner modules from GATK3 (Genome Analysis Toolkit; version 3.5-0) were subsequently used to perform local realignment around indels.

Single nucleotide polymorphism (SNP) identification.   Calling SNPs were performed using the MPileup (version 0.0.1) and Filter pileup (version 1.0.2) tools.

In order to identify SNPs present in the parental line independently of FN treatment or due to mapping error, SNPs retrieved in different sister lines were identified and not considered for further analysis. To generate a list of FN-induced SNPs, only SNPs supported by a coverage of at least four–nine reads corresponding to non-WT alleles were considered in a 'reference population'. Genomic positions corresponding to these FN-induced SNP candidates were investigated in 'MBC population' data using the MPileup (version 0.0.1) and Filter pileup (version 1.0.2) tools. For each position, only SNPs supported by more than 80% of the WT allele were considered as causal FN-induced SNP candidates. The effects of SNPs on protein sequence were investigated using VEP (Variant Effect Predictor) from https://plants.ensembl.org/Arabidopsis_thaliana/Tools/VEP. Silent and intergenic mutations were removed for further analysis.

Indel and chromosome translocation identification.   Indel and chromosome translocation callings were performed using BWA local alignment. Briefly, soft-clipped reads were extracted from the SAM file directly resulting from the mapping step (see above). For each soft-clipped read, the genomic position of the soft-clipped nucleotide in the read was calculated. Genomic positions supported by at least two such soft-clipped genomic sequences were considered as a long-distance genomic rearrangement candidate. Genomic rearrangement candidates were then visually investigated using the Integrative Genomics Viewer (IGV; https://software.broadinstitute.org/software/igv/).

GUS histochemical staining

The GUS staining of Arabidopsis seedlings was conducted as previously described (Balzergue et al., 2017).

Sumoylation assay in *Escherichia coli*

The plasmids encoding the different Arabidopsis proteins of the sumoylation complex, pACYCDuet-AtSAE1b-At-SAE2, pCDFDuet-AtSUMO-AtSCE1 and the control plasmid pET28a-AtMYB30 were kindly provided by Dr K. Tanaka (Okada et al., 2009; Table S3).

We fused the coding sequences of StrepII and HA (haemagglutinin) tags at the 5′-end of the WT *STOP1* sequence by PCR, using the StrepIIHAGlySTOP1Fw and TopoSTOP1stopRv (Table S2) primers. The amplicon was inserted into the entry clone using the pENTR/D-TOPO cloning kit (Invitrogen) in order to yield the StrepII-STOP1WT-pENTRD/topo plasmid. Using this plasmid as a matrix and the primers HA-STOP1-fwd and Ha-STOP1-rev, we PCR amplified *StrepII-HA-STOP1*. The amplicon was then digested with *Kpn*I and *Pac*I, purified on agarose gel and inserted into pETDuet (Novagen) to yield the pETDuet-AtSTOP1 plasmid.

To make the pETDuet-AtSIZ1 plasmid, the full-length coding sequence of *SIZ1* (AT5G60410.2) with codons optimized for expression in *E. coli* (Figure S14) was synthesized (GENEWIZ, www.genewiz.com/) and fused at its 5′-end with a Flag-tag coding sequence, before insertion in a pETDuet plasmid opened with *Xba*I and *Not*I. To make the pETDuet-AtSIZ1-AtSTOP1 plasmid, the AtSIZ1 fragment of the pETDuet-AtSIZ1 plasmid was isolated by digestion with *Xba*I and *Not*I and inserted in pETDuet-AtSTOP1. Proteins produced from these plasmids contain either an N-terminal His-tag (SUMO1, SAE2, MYB30), an N-terminal HA-tag (STOP1), an N-terminal Flag-tag (SIZ1) or a C-terminal S-tag (SCE1, SAE1b).

Escherichia coli BL21(DE3) cells were transformed with pACYCDuet-AtSAE1b-At-SAE2 and/or pCDFDuet-AtSUMO-AtSCE1. Any bacteria containing two plasmids were then rendered competent by $MgCl_2/CaCl_2$ treatment and transformed again with pETDuet-AtSTOP1 or pETDuet-AtSIZ1-AtSTOP1.

Transformed cells were precultured in 10 ml LB medium at 37°C overnight, and used to start a new culture at OD_{600} 0.05 (using the appropriate antibiotics). At OD_{600} 0.6–0.7, IPTG was added to the culture at a final concentration of 0.2 mM. Cells were then grown at 25°C for approximately 12 h and harvested by centrifugation (8000 ***g***, 15 min, 4°C). The cell pellet was resuspended in a 50 mM Tris-HCl pH 7.5 150 mM NaCl buffer and disrupted by sonication on ice with the following cycle: six times for 10 sec with pauses of 45 sec (Fisherbrand™ Sonicator Q500, probe 220B). The supernatant was collected after centrifugation at 10 000 ***g***, 10 min, 4°C. Protein concentration of cell extracts was determined with the CooAssay Protein Dosage Reagent UPF86420 (Uptima/Interchim).

SUMO protease assay

The pET28b derivative encoding the yeast SUMO protease was kindly provided by C. Lima, and the enzyme was purified as previously described (Mossessova and Lima, 2000). After estimating the concentration of the target protein present in the total protein extract using Coomassie blue-stained gels, we added an equivalent amount of SUMO protease and target protein to the sample, after which proteolysis proceeded overnight at room temperature.

Western blot for the sumoylation assay in *Escherichia coli*

Equal amounts of *E. coli* protein extracts were loaded into each lane of an SDS–PAGE (BisTRIS 10% was used and run in MOPS buffer). Five microlitres of the protein ladder (PageRuler™ Prestained Protein Ladder, 10–180 kDa, ThermoFisher) was used. Electrophoresed proteins were blotted onto nitrocellulose membranes and incubated with anti-His horseradish peroxidase (HRP) conjugate (H1029 SIGMA) or anti-HA antibodies (H3663 SIGMA) followed by a secondary anti-mouse HRP conjugate antibody (A9044 SIGMA). Immunoblots were visualized by chemiluminescence (ECL Prime, Dutscher).

Coomassie blue gel staining

The gel was then completely covered in a solution of 0.25% Coomassie Brilliant Blue R-250, 30% methanol and 7% acetic acid for 40 min. Subsequently, it was washed in several baths of 30% ethanol and 7% acetic acid.

Amido black membrane staining

The membrane was washed three times for 10 min in mQ water. The membrane was then completely covered with a solution of 0.1% amido black (w/v) and 10% acetic acid for 40 sec. Finally, it was washed in three successive baths of 5% acetic acid.

Western blots for root tip proteins

Total proteins were extracted by homogenizing an equivalent of four nylon meshes, each containing the frozen root tip of 70–80 seedlings in 70 μl of extraction buffer comprising 50 mM Tris-HCl pH 7.5, 150 mM NaCl, 0.5% Triton X-100 (v/v), 0.5% NP40 (v/v), 0.05% SDS (w/v), 5 mM DTT, 1 × cOmplete protease inhibitor cocktail (Roche), 100 μM MG-132, 20 mM NEM and 1 × PhosSTOP cocktail (Roche). Extracts were centrifuged twice at 20 000 **g** for 15 min at 4°C, and protein concentration was determined using the 2D Quant kit (GE Healthcare). For each sample, 20 μg of proteins was separated on a 10% acrylamide Bis-Tris gel using MOPS running buffer. Resolved proteins were transferred for 10 min on a nitrocellulose membrane using the Trans-Blot Turbo transfer system (Bio-Rad). Membranes were incubated overnight at 4°C in phosphate-buffered saline (PBS) buffer containing 0.1% Tween (v/v) and 5% non-fat milk (w/v), henceforth called PBS-T + milk. To detect GFP-STOP1, blots were incubated for 1 h in HRP-conjugated anti-GFP antibodies (SC-9996 HRP, Santa Cruz Biotechnology) diluted (1:5000) in PBS-T + milk. To detect GAPC, blots were incubated for 1 h in anti-GAPC1/2 antibodies (AS15 2894, Agrisera) diluted (1:10 000) in PBS-T + milk. Blots were washed three times for 10 min in PBS, PBS-T and PBS before 1 h incubation with secondary anti-rabbit HRP-conjugated antibodies diluted (1:10 000) in PBS-T + milk. Blots were washed again as previously described, and chemiluminescent signals were detected using a G/BOX system (Syngene). Densitometry analyses were performed using the ImageJ software (Rasband, 1997-2016). For each sample, GFP signals were normalized by GAPC signals and expressed as arbitrary units.

CONFLICT OF INTEREST

The authors declare that they have no conflicts of interest.

SUPPORTING INFORMATION

Additional Supporting Information may be found in the online version of this article.

Figure S1. Images of *sup33-46*, *sup33-90* and *siz1-3* mutants, with the WT and *stop1^33* controls.
Figure S2. Primary root length of the backcross F2 populations of *sup33* mutants.
Figure S3. PCR genotyping of the *sup33* mutations.
Figure S4. Position of the *sup33* and *siz1-3* mutations on the protein map of SIZ1 (amino acids).
Figure S5. Images of plants homozygous for *stop1^33* (a) or *stop1^127* (b) selected in the F2 progeny of the genetic cross of *siz1-3* with *stop1^33* or *stop1^127*.
Figure S6. Genotyping of 24 F2 plants from the cross *stop1^33* X *siz1-3*.
Figure S7. Allelism tests.
Figure S8. Primary root length of seedlings grown with or without Al^{3+}.
Figure S9. Primary root length of seedlings grown under −Pi.
Figure S10. Production of the four proteins of the Arabidopsis sumoylation complex in *E. coli*.
Figure S11. Protein loading controls for Figure 5.
Figure S12. Purified *Saccharomyces cerevisiae* His-tagged SUMO protease used in the SUMO protease assay.
Figure S13. Protein loading controls for Figure 6.
Figure S14. DNA sequence of *SIZ1* in the pETDuet-AtSIZ1 and pETDuet-AtSIZ1-AtSTOP1 plasmids.
Figure S15. Expression of SIZ1 with the Arabidopsis core sumoylation complex in *Escherichia coli* and in the presence of STOP1.
Figure S16. Uncropped images from Figure 7a.
Table S1. Elemental composition of the agar.
Table S2. List of primers.
Table S3. List of plasmids.

REFERENCES

Abel, S. (2017) Phosphate scouting by root tips. *Current Opinion in Plant Biology*, **39**, 168–177.

Augustine, R.C. & Vierstra, R.D. (2018) SUMOylation: re-wiring the plant nucleus during stress and development. *Current Opinion in Plant Biology*, **45**, 143–154.

Balzergue, C., Dartevelle, T., Godon, C., Laugier, E., Meisrimler, C., Teulon, J.M. et al. (2017) Low phosphate activates STOP1-ALMT1 to rapidly inhibit root cell elongation. *Nature Communications*, **8**, 15300.

Belfield, E.J., Gan, X.C., Mithani, A., Brown, C., Jiang, C.F., Franklin, K. et al. (2012) Genome-wide analysis of mutations in mutant lineages selected following fast-neutron irradiation mutagenesis of Arabidopsis thaliana. *Genome Research*, **22**, 1306–1315.

Benlloch, R. & Lois, L.M. (2018) Sumoylation in plants: mechanistic insights and its role in drought stress. *Journal of Experimental Botany*, **69**(19), 4539–4554.

Bustos, R., Castrillo, G., Linhares, F., Puga, M.I., Rubio, V., Perez-Perez, J. et al. (2010) A central regulatory system largely controls transcriptional activation and repression responses to phosphate starvation in Arabidopsis. *PLoS Genetics*, **6**, e1001102.

Castro, P.H., Tavares, R.M., Bejarano, E.R. & Azevedo, H. (2012) SUMO, a heavyweight player in plant abiotic stress responses. *Cellular and Molecular Life Sciences*, **69**, 3269–3283.

Daspute, A.A., Sadhukhan, A., Tokizawa, M., Kobayashi, Y., Panda, S.K. & Koyama, H. (2017) Transcriptional regulation of aluminum-tolerance genes in higher plants: clarifying the underlying molecular mechanisms. *Frontiers in Plant Science*, **8**, 1358.

Elrouby, N. & Coupland, G. (2010) Proteome-wide screens for small ubiquitin-like modifier (SUMO) substrates identify Arabidopsis proteins implicated in diverse biological processes. *Proceedings of the National Academy of Sciences of the United States of America*, **107**, 17415–17420.

Fang, Q., Zhang, J., Yang, D.-L. & Huang, C.-F. (2021a) The SUMO E3 ligase SIZ1 partially regulates STOP1 SUMOylation and stability in Arabidopsis thaliana. *Plant Signaling & Behavior*, **16**, 1899487.

Fang, Q., Zhang, J., Zhang, Y., Fan, N., van den Burg, H.A. & Huang, C.F. (2020) Regulation of aluminum resistance in Arabidopsis involves the SUMOylation of the zinc finger transcription factor STOP1. *The Plant Cell*, **32**, 3921–3938.

Fang, Q., Zhou, F., Zhang, Y., Singh, S. & Huang, C.F. (2021b) STOP1 degradation mediated by the F-box proteins RAH1 and RAE1 balances aluminum resistance and plant growth in Arabidopsis thaliana. *The Plant Journal*, **106**(2), 493–506.

Flotho, A. & Melchior, F. (2013) Sumoylation: a regulatory protein modification in health and disease. *Annual Review of Biochemistry*, **82**(82), 357–385.

Garcia-Dominguez, M., March-Diaz, R. & Reyes, J. (2008) The PHD domain of plant PIAS proteins mediates sumoylation of bromodomain GTE proteins. *Journal of Biological Chemistry*, **283**, 21469–21477.

Godon, C., Mercier, C., Wang, X., David, P., Richaud, P., Nussaume, L. et al. (2019) Under phosphate starvation conditions, Fe and Al trigger accumulation of the transcription factor STOP1 in the nucleus of Arabidopsis root cells. *The Plant Journal*, **99**, 937–949.

Guo, J., Zhang, Y., Gao, H., Li, S., Wang, Z.-Y. & Huang, C.-F. (2020) Mutation of HPR1 encoding a component of the THO/TREX complex reduces STOP1 accumulation and aluminium resistance in Arabidopsis thaliana. *New Phytologist*, **228**, 179–193.

Gutiérrez-Alaniís, D., Ojeda-Rivera, J.O., Yong-Villalobos, L., Cárdenas-Torres, L. & Herrera-Estrella, L. (2018) Adaptation to phosphate scarcity: tips from Arabidopsis roots. *Trends in Plant Science*, **23**, 721–730.

Gutiérrez-Alanís, D., Yong-Villalobos, L., Jiménez-Sandoval, P., Alatorre-Cobos, F., Oropeza-Aburto, A., Mora-Macías, J. et al. (2017) Phosphate starvation-dependent iron mobilization induces CLE14 expression to trigger root meristem differentiation through CLV2/PEPR2 signaling. *Developmental Cell*, **41**, 555–570.

Hietakangas, V., Anckar, J., Blomster, H.A., Fujimoto, M., Palvimo, J.J., Nakai, A. et al. (2006) PDSM, a motif for phosphorylation-dependent SUMO modification. *Proceedings of the National Academy of Sciences of the United States of America*, **103**, 45–50.

Hoekenga, O.A., Maron, L.G., Piñeros, M.A., Cançado, G.M., Shaff, J., Kobayashi, Y. et al. (2006) AtALMT1, which encodes a malate transporter, is identified as one of several genes critical for aluminum tolerance in Arabidopsis. *Proceedings of the National Academy of Sciences of the United States of America*, **103**, 9738–9743.

Iuchi, S., Koyama, H., Iuchi, A., Kobayashi, Y., Kitabayashi, S., Kobayashi, Y. et al. (2007) Zinc finger protein STOP1 is critical for proton tolerance in Arabidopsis and coregulates a key gene in aluminum tolerance. *Proceedings of the National Academy of Sciences of the United States of America*, **104**, 9900–9905.

Jiang, F., Wang, T., Wang, Y.Q., Kochian, L.V., Chen, F. & Liu, J.P. (2017) Identification and characterization of suppressor mutants of stop1. *BMC Plant Biology*, **17**(1), 128.

Kim, D.Y., Han, Y.J., Kim, S.I., Song, J.T. & Seo, H.S. (2015a) Arabidopsis CMT3 activity is positively regulated by AtSIZ1-mediated sumoylation. *Plant Science*, **239**, 209–215.

Kim, S.I., Park, B.S., Kim, D.Y., Yeu, S.Y., Song, S.I., Song, J.T. et al. (2015b) E3 SUMO ligase AtSIZ1 positively regulates SLY1-mediated GA signalling and plant development. *Biochemical Journal*, **469**(2), 299–314.

Kobayashi, Y., Hoekenga, O.A., Itoh, H., Nakashima, M., Saito, S., Shaff, J.E. et al. (2007) Characterization of AtALMT1 expression in aluminum-inducible malate release and its role for rhizotoxic stress tolerance in Arabidopsis. *Plant Physiology*, **145**, 843–852.

Kochian, L.V., Pineros, M.A., Liu, J.P. & Magalhaes, J.V. (2015) Plant adaptation to acid soils: the molecular basis for crop aluminum resistance. *Annual Review of Plant Biology*, **66**, 571–598.

Lee, J., Nam, J., Park, H.C., Na, G., Miura, K., Jin, J.B. et al. (2007) Salicylic acid-mediated innate immunity in Arabidopsis is regulated by SIZ1 SUMO E3 ligase. *Plant Journal*, **49**, 79–90.

Liu, C., Yu, H. & Li, L.G. (2019) SUMO modification of LBD30 by SIZ1 regulates secondary cell wall formation in Arabidopsis thaliana. *PLoS Genetics*, **15**, e1007928.

Liu, J., Magalhaes, J.V., Shaff, J. & Kochian, L.V. (2009) Aluminum-activated citrate and malate transporters from the MATE and ALMT families function independently to confer Arabidopsis aluminum tolerance. *The Plant Journal*, **57**, 389–399.

Mazur, M.J., Spears, B.J., Djajasaputra, A., van der Gragt, M., Vlachakis, G., Beerens, B. et al. (2017) Arabidopsis TCP Transcription Factors Interact with the SUMO Conjugating Machinery in Nuclear Foci. *Frontiers in Plant Science*, **8**, 2043.

Mergner, J., Frejno, M., List, M., Papacek, M., Chen, X., Chaudhary, A. et al. (2020) Mass-spectrometry-based draft of the Arabidopsis proteome. *Nature*, **579**, 409–414.

Miller, M.J., Barrett-Wilt, G.A., Hua, Z.H. & Vierstra, R.D. (2010) Proteomic analyses identify a diverse array of nuclear processes affected by small ubiquitin-like modifier conjugation in Arabidopsis. *Proceedings of the National Academy of Sciences of the United States of America*, **107**, 16512–16517.

Miller, M.J., Scalf, M., Rytz, T.C., Hubler, S.L., Smith, L.M. & Vierstra, R.D. (2013) Quantitative proteomics reveals factors regulating RNA biology as dynamic targets of stress-induced SUMOylation in Arabidopsis. *Molecular & Cellular Proteomics*, **12**, 449–463.

Miura, K. & Hasegawa, P.M. (2010) Sumoylation and other ubiquitin-like post-translational modifications in plants. *Trends in Cell Biology*, **20**, 223–232.

Miura, K., Jin, J.B., Lee, J., Yoo, C.Y., Stirm, V., Miura, T. et al. (2007) SIZ1-mediated sumoylation of ICE1 controls CBF3/DREB1A expression and freezing tolerance in Arabidopsis. *The Plant Cell*, **19**, 1403–1414.

Miura, K., Lee, J., Gong, Q., Ma, S., Jin, J.B., Yoo, C.Y. et al. (2011) SIZ1 regulation of phosphate starvation-induced root architecture remodeling involves the control of auxin accumulation. *Plant Physiology*, **155**, 1000–1012.

Miura, K., Lee, J., Jin, J.B., Yoo, C.Y., Miura, T. & Hasegawa, P.M. (2009) Sumoylation of ABI5 by the Arabidopsis SUMO E3 ligase SIZ1 negatively regulates abscisic acid signaling. *Proceedings of the National Academy of Sciences of the United States of America*, **106**, 5418–5423.

Miura, K., Rus, A., Sharkhuu, A., Yokoi, S., Karthikeyan, A.S., Raghothama, K.G. et al. (2005) The Arabidopsis SUMO E3 ligase SIZ1 controls phosphate deficiency responses. *Proceedings of the National Academy of Sciences of the United States of America*, **102**, 7760–7765.

Mora-Macias, J., Ojeda-Rivera, J.O., Gutierrez-Alanis, D., Yong-Villalobos, L., Oropeza-Aburto, A., Raya-Gonzalez, J. et al. (2017) Malate-dependent

Fe accumulation is a critical checkpoint in the root developmental response to low phosphate. *Proceedings of the National Academy of Sciences of the United States of America*, **114**, E3563–E3572.

Mossessova, E. & Lima, C.D. (2000) Ulp1-SUMO crystal structure and genetic analysis reveal conserved interactions and a regulatory element essential for cell growth in yeast. *Molecular Cell*, **5**, 865–876.

Muller, J., Toev, T., Heisters, M., Teller, J., Moore, K.L., Hause, G. et al. (2015) Iron-dependent callose deposition adjusts root meristem maintenance to phosphate availability. *Developmental Cell*, **33**, 216–230.

Niu, Y.F., Chai, R.S., Jin, G.L., Wang, H., Tang, C.X. & Zhang, Y.S. (2013) Responses of root architecture development to low phosphorus availability: a review. *Annals of Botany*, **112**, 391–408.

Novatchkova, M., Tomanov, K., Hofmann, K., Stuible, H.-P. & Bachmair, A. (2012) Update on sumoylation: defining core components of the plant SUMO conjugation system by phylogenetic comparison. *New Phytologist*, **195**(1), 23–31.

Okada, S., Nagabuchi, M., Takamura, Y., Nakagawa, T., Shinmyozu, K., Nakayama, J. et al. (2009) Reconstitution of Arabidopsis thaliana SUMO pathways in E-coli: functional evaluation of SUMO machinery proteins and mapping of SUMOylation sites by mass spectrometry. *Plant and Cell Physiology*, **50**(6), 1049–1061.

Rasband, W. (1997–2016) *ImageJ* [Online]. National Institutes of Health. Bethesda, Maryland, USA. Available: http://imagej.nih.gov/ij/

Raya-González, J., Ojeda-Rivera, J.O., Mora-Macias, J., Oropeza-Aburto, A., Ruiz-Herrera, L.F., López-Bucio, J. et al. (2020) MEDIATOR16 orchestrates local and systemic responses to phosphate scarcity in Arabidopsis roots. *New Phytologist*, **229**(3), 1278–1288.

Rubio, V., Linhares, F., Solano, R., Martin, A.C., Iglesias, J., Leyva, A. et al. (2001) A conserved MYB transcription factor involved in phosphate starvation signaling both in vascular plants and in unicellular algae. *Genes & Development*, **15**, 2122–2133.

Rytz, T.C., Miller, M.J., McLoughlin, F., Augustine, R.C., Marshall, R.S., Juan, Y.T. et al. (2018) SUMOylome profiling reveals a diverse array of nuclear targets modified by the SUMO ligase SIZ1 during heat stress. *The Plant Cell*, **30**, 1077–1099.

Saracco, S.A., Miller, M.J., Kurepa, J. & Vierstra, R.D. (2007) Genetic analysis of SUMOylation in arabidopsis: Conjugation of SUMO1 and SUMO2 to nuclear proteins is essential. *Plant Physiology*, **145**, 119–134.

Sawaki, Y., Iuchi, S., Kobayashi, Y., Ikka, T., Sakurai, N., Fujita, M. et al. (2009) STOP1 regulates multiple genes that protect arabidopsis from proton and aluminum toxicities. *Plant Physiology*, **150**, 281–294.

Svistoonoff, S., Creff, A., Reymond, M., Sigoillot-Claude, C., Ricaud, L., Blanchet, A. et al. (2007) Root tip contact with low-phosphate media reprograms plant root architecture. *Nature Genetics*, **39**, 792–796.

Thibaud, M.C., Arrighi, J.F., Bayle, V., Chiarenza, S., Creff, A., Bustos, R. et al. (2010) Dissection of local and systemic transcriptional responses to phosphate starvation in Arabidopsis. *The Plant Journal*, **64**, 775–789.

Ticconi, C.A., Lucero, R.D., Sakhonwasee, S., Adamson, A.W., Creff, A., Nussaume, L. et al. (2009) ER-resident proteins PDR2 and LPR1 mediate the developmental response of root meristems to phosphate availability. *Proceedings of the National Academy of Sciences of the United States of America*, **106**, 14174–14179.

Tokizawa, M., Enomoto, T., Ito, H., Wu, L., Kobayashi, Y., Mora-Macías, J. et al. (2021) High affinity promoter binding of STOP1 is essential for the early aluminum-inducible expression of novel Al resistance genes GDH1 and GDH2 in Arabidopsis. *Journal of Experimental Botany*, **72**(7), 2769–2789.

Tomanov, K., Nukarinen, E., Vicente, J., Mendiondo, G.M., Winter, N., Nehlin, L. et al. (2018) Sumoylation and phosphorylation: hidden and overt links. *Journal of Experimental Botany*, **69**, 4583–4590.

Vu, L.D., Gevaert, K. & de Smet, I. (2018) Protein language: post-translational modifications talking to each other. *Trends in Plant Science*, **23**, 1068–1080.

Wang, X., Wang, Z., Zheng, Z., Dong, J., Song, L., Sui, L. et al. (2019) Genetic dissection of Fe-dependent signaling in root developmental responses to phosphate deficiency. *Plant Physiology*, **179**, 300–316.

Weigel, D. & Glazebrook, J. (2002) *Arabidopsis: A Laboratory Manual*. Cold Spring Harbor, NY: Cold Spring Harbor Laboratory Press.

Xu, J.M., Zhu, J.Y., Liu, J.J., Wang, J.X., Ding, Z.J. & Tian, H.Y. (2021) SIZ1 negatively regulates aluminum resistance by mediating the STOP1-ALMT1 pathway in Arabidopsis. *Journal of Integrative Plant Biology*, **63**, 1147–1160.

Zhang, L.E., Han, Q., Xiong, J.W., Zheng, T., Han, J.F., Zhou, H.B. et al. (2019a) Sumoylation of BRI1-EMS-SUPPRESSOR 1 (BES1) by the SUMO E3 ligase SIZ1 negatively regulates brassinosteroids signaling in Arabidopsis thaliana. *Plant and Cell Physiology*, **60**(10), 2282–2292.

Zhang, X., Huai, J., Liu, S., Jin, J. & Lin, R. (2020) SIZ1-Mediated SUMO Modification of SEUSS Regulates Photomorphogenesis in Arabidopsis. *Plant Communications*, **1**.

Zhang, Y., Zhang, J., Guo, J., Zhou, F., Singh, S., Xu, X. et al. (2019b) F-box protein RAE1 regulates the stability of the aluminum-resistance transcription factor STOP1 in Arabidopsis. *Proceedings of the National Academy of Sciences of the United States of America*, **116**(1), 319–327.

Zheng, Y., Schumaker, K.S. & Guo, Y. (2012) Sumoylation of transcription factor MYB30 by the small ubiquitin-like modifier E3 ligase SIZ1 mediates abscisic acid response in Arabidopsis thaliana. *Proceedings of the National Academy of Sciences of the United States of America*, **109**, 12822–12827.